MATERIALS SCIENCE

3D touchless multiorder reflection structural color sensing display

Han Sol Kang[1], Sang Won Han[2], Chanho Park[1], Seung Won Lee[1], Hongkyu Eoh[1], Jonghyeok Baek[3], Dong-Gap Shin[3], Tae Hyun Park[1], June Huh[4], Hyungsuk Lee[3], Dae-Eun Kim[3], Du Yeol Ryu[2], Edwin L. Thomas[5], Won-Gun Koh[2]*, Cheolmin Park[1,6]*

The development of a lightweight, low-power, user-interactive three-dimensional (3D) touchless display in which a human stimulus can be detected and simultaneously visualized in noncontact mode is of great interest. Here, we present a user-interactive 3D touchless sensing display based on multiorder reflection structural colors (SCs) of a thin, solid-state block copolymer (BCP) photonic crystal (PC). Full-visible-range SCs are developed in a BCP PC consisting of alternating lamellae, one of which contains a chemically cross-linked, interpenetrated hydrogel network. The absorption of a nonvolatile ionic liquid into the domains of the interpenetrated network allows for further manipulation of SC by using multiple-order photonic reflections, giving rise to unprecedented visible SCs arising from reflective color mixing. Furthermore, by using a hygroscopic ionic liquid ink, a printable 3D touchless interactive display is created where 3D position of a human finger is efficiently visualized in different SCs as a function of finger-to-display distance.

INTRODUCTION

User-interactive displays (UIDs) that allow for visualization of sensible but invisible information such as touch, smell, and sound are of great interest with their potentials in emerging wearable and patchable electronics for upcoming hyperconnected society (*1*, *2*). In particular, owing to the tremendous demand for electronic skin (e-skins) that can artificially mimic the properties of human skin such as sensing pressure, temperature, and humidity, a variety of the human-interactive touch displays have been demonstrated by visualizing local changes in pressure (*3*–*6*), temperature (*7*), and humidity (*8*). Diverse optical elements were used for the development of touch interactive displays including light-emitting diodes (LEDs) (*5*, *7*, *9*), electrochromic (*10*, *11*), thermochromic (*12*), and triboelectrification devices (*13*, *14*), and alternating current (AC)–driven electroluminescent devices (*5*, *7*, *9*, *15*, *16*). Despite great progress in UIDs, most of the displays are based on the variation in intensity of light emission or chromic reflection as a function of the degree of a stimulus. A change in color with a variation of a stimulus may be more favorable, allowing for more distinct stimulus visualization. A touchless platform is in great demand for three-dimensional (3D) interactive touch displays where visualization of a stimulus can occur in noncontact mode and color can vary with distance of the stimulus from the platform. We envision that low-power reflective-mode visible-range structural color (SC) of a stimuli-interactive photonic crystal (PC) can satisfy the aforementioned requirements, giving rise to a user-interactive 3D touchless display (*3*, *4*, *6*, *17*–*29*).

We use SCs arising from self-assembled 1D block copolymer (BCP) PCs, whose layered 1D periodic microstructure spontaneously develops upon film formation. It is possible to tune the dielectric constants of the layers by a number of diverse external and environmental forces (*6*, *18*, *19*, *23*–*29*), and here, we present a 3D touchless interactive display. To ensure a solid-state, full-visible-range SC BCP PC, we develop chemically cross-linked interpenetrated hydrogel network (IHN) layers in a BCP PC microdomain. The SC of such a BCP PC with an effective modulus of approximately 500 MPa is readily controlled by infusing various amounts of poly(ethylene glycol diacetate) (PEGDA) oligomers into quaternized 2-vinyl pyridine (Q2VP) layers and then chemically cross-linking the precursors through ultraviolet (UV) exposure. Moreover, when a nonvolatile ionic liquid is subsequently absorbed into the Q2VP-PEGDA domains of the interpenetrated network, the BCP SC is further controlled with not only first-order but also second- and third-order photonic reflections, giving rise to richer visible SCs arising from reflective color mixing. Furthermore, by using the ionic liquid as an ink for ink-jet printing, a variety of full SC display images can be instantly produced. Thus, a printable 3D touchless interactive display is realized by using a hygroscopic ionic liquid ink, which allows facile SC variation as a function of humidity. We demonstrated 3D position sensing of the water vapor emanating from a human finger as a function of finger-to-film distance, making our device suitable for various emerging wearable electronic applications.

RESULTS

A 700-nm-thick polystyrene-block-poly(2-vinylpyridine) (PS-*b*-P2VP) film, comprising alternating in-plane ordered PS and P2VP lamellae, was formed by spin coating a BCP solution in propylene glycol monomethyl acetate (PGMEA) onto a glass substrate. Then, the film was solvent annealed with chloroform vapor at 60°C for 24 hours to develop a well-defined in-plane orientation of parallel lamellae. The P2VP blocks were subsequently quaternized by soaking the BCP film in 1-bromoethane solution (solvent: hexane) for

[1]Department of Materials Science and Engineering, Yonsei University, Seoul 03722, Republic of Korea. [2]Department of Chemical and Biomolecular Engineering, Yonsei University, Seoul 03722, Republic of Korea. [3]School of Mechanical Engineering, Yonsei University, Seoul 03722, Republic of Korea. [4]Department of Chemical and Biological Engineering, Korea University, Seoul 02841, Republic of Korea. [5]Material Science and Nano Engineering, Rice University, Houston, TX 77005-1892, USA. [6]Spin Convergence Research Center, Korea Institute of Science and Technology (KIST), Seoul 02792, Republic of Korea.
*Corresponding author. Email: cmpark@yonsei.ac.kr (C.P.); wongun@yonsei.ac.kr (W.-G.K.)

24 hours. After the film was completely dried, a mixture of PEGDA oligomer, 2-hydroxy-2-methylpropiophenone (HOMPP), and Triton X in deionized (DI) water was spread onto the surface of the film, allowing the solution to preferentially diffuse into and swell the quaternized poly(2-vinylpyridine) (QP2VP) domains. The BCP film with the hydrogel oligomer and initiator was then irradiated with UV (a wavelength of 350 nm) for various exposure times (10 to 60 s), followed by rinsing and removal of the unreacted residual oligomer, giving rise to an IHN in the QP2VP domains, as shown in Fig. 1A (fig. S1A).

The amount of IHN in the QP2VP domains was readily controlled by the UV irradiation time because the amount of extractable

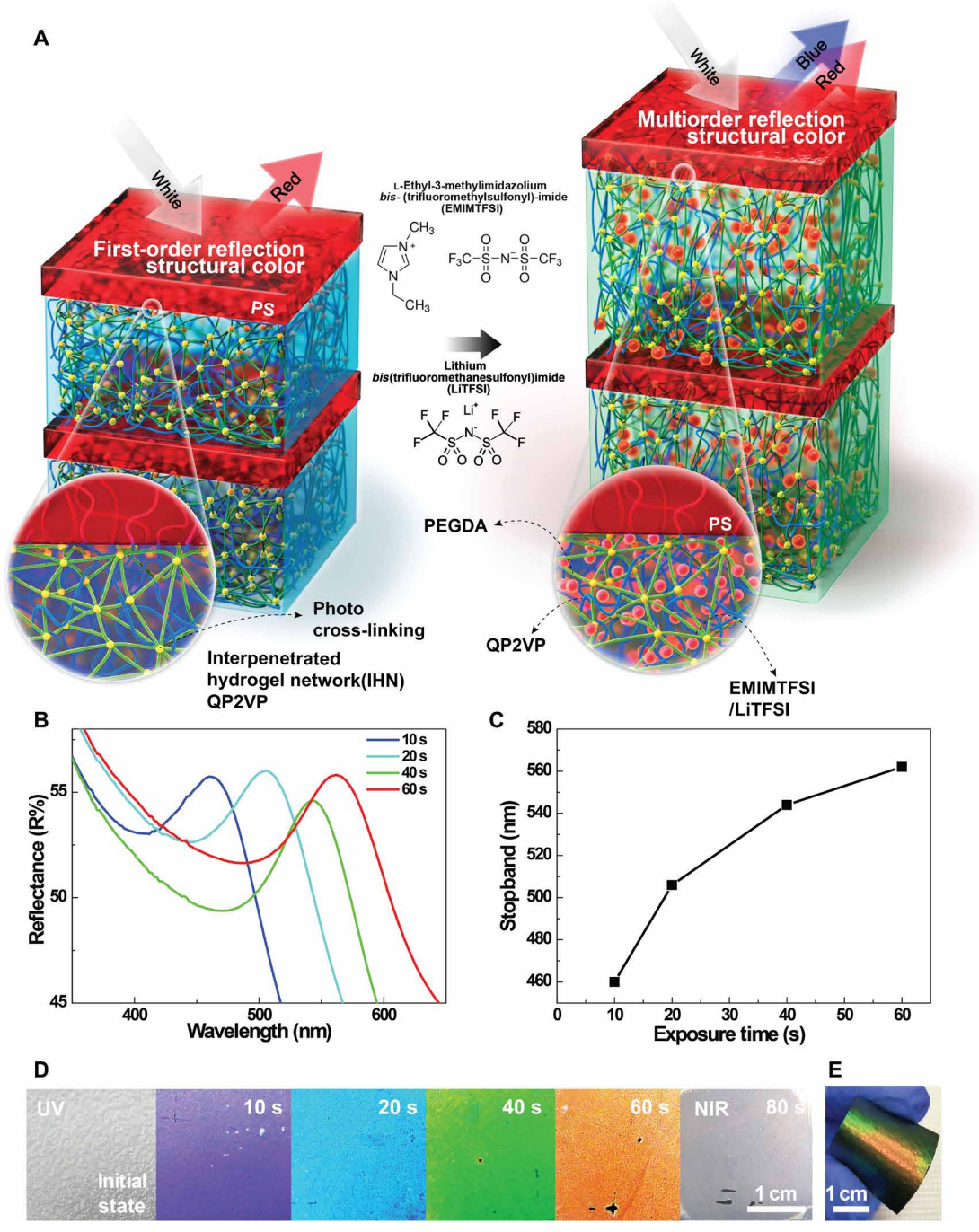

Fig. 1. Interpenetrated hydrogel network block copolymer photonic crystal. (**A**) Schematic illustration of BCP PC display with multiorder reflection SCs. Visible range SC of BCP PC is realized with the interpenetrated hydrogel network (IHN) of PEGDA in PQ2VP domains. By using nonvolatile ionic liquid of either EMITFSI or LiTFSI in IHN BCP PC, richer SCs are developed by mixing of multiorder reflection SCs. (**B**) Ultraviolet-visible (UV-vis) spectra of IHN BCP PC films on the glass as a function of UV exposure time. (**C**) Plot of the wavelength at maximum reflection as a function of UV exposure time from 10 to 60 s. (**D**) Photographs of IHN BCP PC film on glass substrates as a function of UV exposure time. The right end photograph shows its maximum reflection in near infrared (NIR) regime. (**E**) Photographs of a solid-like flexible IHN BCP PC on a black paper. Photo credit: H.S.K., Yonsei University.

oligomer decreased with the irradiation, increasing the IHN-QP2VP domain thickness after washing and oligomer extraction. As a consequence, the stopband of a BCP PC with IHN-QP2VP domains was red shifted with UV dose, as shown in Fig. 1B. The wavelengths at the maximum reflectance increased with the UV irradiation time, giving rise to a BCP PC with IHN-QP2VP domains (IHN BCP PC), capable of controlling its SC across the full visible range, as shown in Fig. 1C. The irradiation time–dependent SC variation is demonstrated with photographs of IHN BCP PCs in Fig. 1D. Our PS-*b*-QP2VP-IHN BCP PC is pseudoelastic, with excellent mechanical robustness, flexibility, without sticky, gel-like viscoelasticity on its upper surface, as shown in Fig. 1E, making the material suitable for a solid-state sensing display as shown later.

The self-assembled solid-state IHN BCP PC was characterized with both grazing incident small angle x-ray scattering (GISAXS) and transmission electron microscopy (TEM), and the results are shown in Fig. 2. First, we used GISAXS to reveal the periodic order of the in-plane lamellar structures of IHN BCP PCs with the representative blue (B), green (G), and red (R) 1D periodic SCs, which were prepared via the different UV irradiation times of 10, 40, and 60 s, respectively. The 2D GISAXS patterns obtained from the IHN BCP PC films with the B, G, and R SCs in Fig. 2, A to C, respectively, show multiple orders of sharp spot-like multiple reflections along the meridian (q_z), indicating the development of highly ordered 1D PC structures. Plots of the scattered intensity along the q_z direction clearly exhibit the characteristic q_n/q_1 ratios of 1, 2, 3, and 4 of lamellae. It should be noted that the first-order reflections of the G and R samples, expected at q_z of 0.03 and 0.05 nm^{-1}, respectively, were barely observed because the beam stop abstracted these q_z regions. On the basis of both observed and expected q_1 values, the

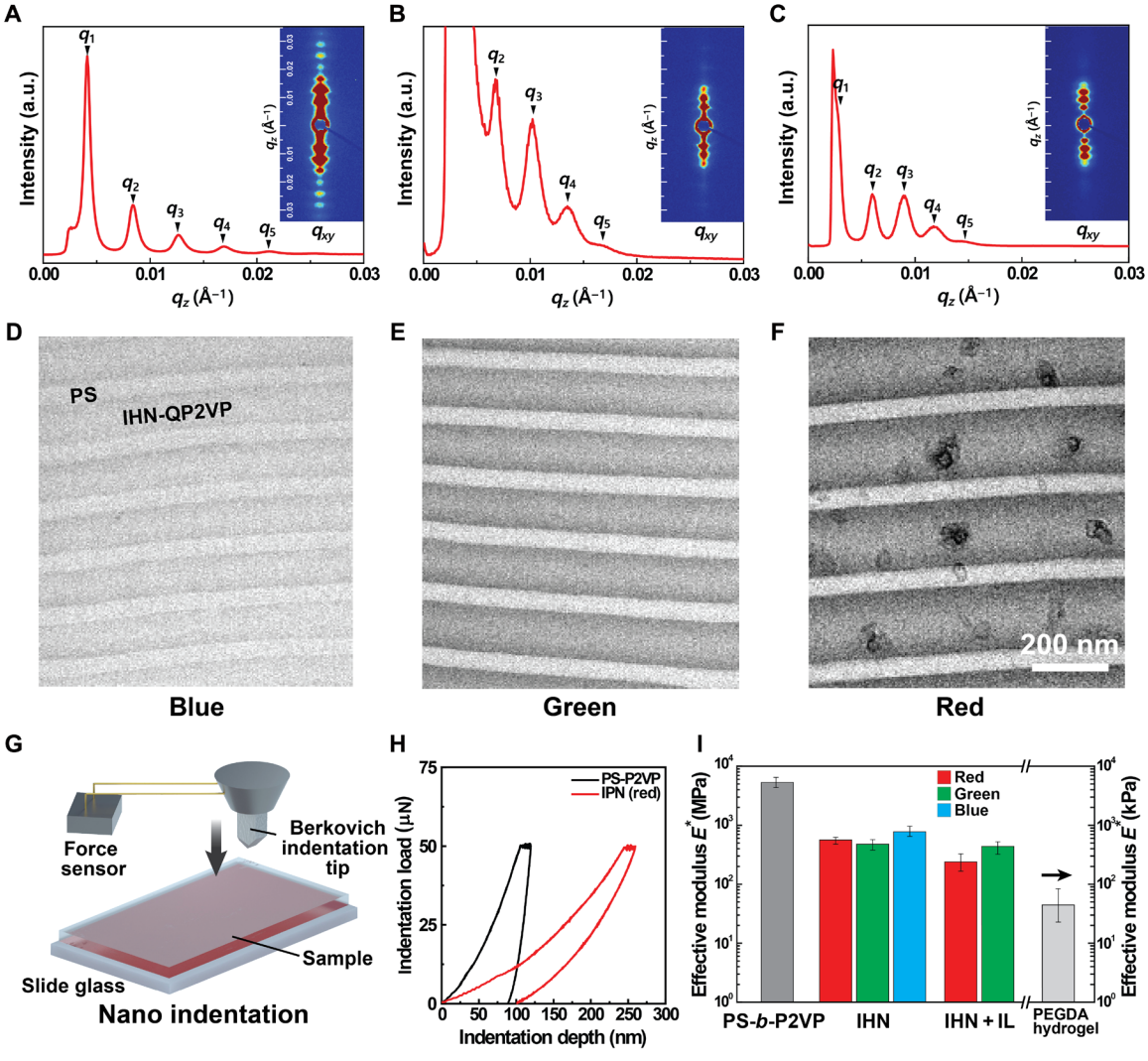

Fig. 2. Structural and mechanical properties of IHN BCP PC. (**A** to **C**) Scattering intensity versus q_z plots of IHN BCP PC films with different SCs of blue, green, and red, based on 2D GISAXS results in the insets. a.u., arbitrary unit. From left to right: Cross-sectional bright-field TEM images of IHN BCP PC films with different SCs of (**D**) blue (lamellae periodicity 151 nm), (**E**) green (lamellae periodicity 181 nm), and (**F**) red (lamellae periodicity 203 nm). From left to right: (**G**) Schematic illustration of nanoindentation experiment performed with the sequential loading, holding, and unloading. (**H**) Force-distance curves of the PS-*b*-P2VP and IHN BCP PC with red SC. (**I**) Effective moduli of a PS-*b*-P2VP, IHN BCP PCs with different SCs of blue, green, and red, and IHN BCP PCs with different amounts of EMITFSI. Effective modulus of a bare PEGDA hydrogel is also shown on the right side.

periodicities of the in-plane lamellae of the three IHN BCP PCs were calculated as approximately 151, 181, and 203 nm, respectively, consistent with simulation results by the finite-difference time-domain (FDTD) method (fig. S2) (*30*).

The self-assembled nanostructures of the IHN BCP PCs could be directly visualized with cross-sectional TEM, and the results are shown in Fig. 2, D to F. Our mechanically robust films were readily cross-sectioned with a focused ion beam (FIB), followed by preferential staining the IHN-QP2VP domains with iodine (I_2). Asymmetric thickness PS (45 nm) and IHN-QP2VP (106 to 158) lamellae were observed in layers, while near symmetric alternating PS/QP2VP lamellae were obtained in a neat PS-*b*-QP2VP film, as shown in Fig. 2, D and E. The results suggest that IHN preferentially locates within the QP2VP domains, allowing for an effective thickness increase of the IHN-QP2VP domain, while the glassy PS domains retain their 45-nm thickness. The B, G, and R films have IHN-QP2VP domains of approximately 105, 135, and 158 nm in thickness, with corresponding 1D periodicities of 150, 180, and 203 nm, respectively, consistent with those obtained with GISAXS (Fig. 2, A to C). The dark dots observed in Fig. 2F result from slight contamination of the cross-sectioned sample during TEM measurement. Consistent with our previous work (*23*), our BCP films also showed the screw dislocations distributed on the surface with the size of approximately 5 mm in diameter (fig. S1B). These screw dislocations facilitated the transport of the liquid and oligomeric agents into the BCP film. The water molecule is diffused mostly through the screw dislocations present in the BCP film, which means that the water diffusion is dominantly longitudinal rather than transverse through in-plane diffusion.

The *z* axis mechanical properties of our IHN BCP PCs were examined using nanoindentation, as schematically shown in Fig. 2G. The indentation experiment was performed with sequential loading, holding, and unloading, with a holding interval time of 60 s to minimize the noise arising from the viscoelasticity of a polymer (fig. S3). Speeds of both approach and retraction were approximately 2 nm s^{-1}. To minimize the possible contribution of the substrate, the indentation depth was smaller than 10% of the film thickness. The Berkovich tip was used with a three-sided pyramid shape (a tip radius ~10 nm). An effective modulus of an IHN BCP PC film was estimated by fitting the force-indentation depth curves obtained during unloading (Fig. 2H) to the Oliver and Pharr model (*31*, *32*), followed by $\frac{dP}{dh}|_{h=h_{max}} = 1.034 \cdot \frac{2}{\sqrt{\pi}} \cdot E_{eff} \cdot \sqrt{A}$, where P, h_{max}, E_{eff}, and A are applied force, indentation depth, maximum indentation depth, effective elastic modulus, and contact area, respectively. The compressive modulus of a PS-*b*-P2VP film was evaluated to be approximately 5.3 GPa, as shown in Fig. 2I. The modulus is as expected, similar to those observed for conventional glassy polymers such as PS and P2VP. The addition of PEGDA, and water making an interpenetrating hydrogel having an effective modulus of a few MPa, into QP2VP domains greatly reduced the effective modulus (*33*), and thus, IHN BCP PCs with full-visible-range SC exhibited moduli an order of magnitude lower of 300 to 500 MPa, as shown in Fig. 2I. No distinct dependency of the effective modulus on layer swelling within experimental uncertainty was, however, observed, although the largest amount of IHN was involved in an IHN BCP PC with red SC. It should be noted that our IHN BCP PCs are pseudoelastic without notable hysteresis in indentation load-depth curve frequently observed in numerous viscoelastic systems (*32*). Furthermore, the effective modulus values of B, G, and R IHN BCP PCs are a few orders of magnitude greater than those of PCs based on hydrogels ranging from a few to tens of kPa (*34*, *35*).

SCs of our IHN BCP PCs with the pseudoelastic properties were further modulated by adding a nonvolatile ionic liquid swelling agent in an IHN BCP PC, giving rise to richer visible-range SCs arising from the color mixing of higher-order photonic reflections, as schematically shown in Fig. 1A. The experimental results are shown in Fig. 3. We chose L-ethyl-3-methylimidazolium *bis*-(trifluoromethylsulfonyl)-imide (EMIMTFSI) as a nonvolatile and least-hygroscopic-swelling agent, which could avoid possible influence by water molecules associated with the ionic liquid (fig. S4A). To demonstrate the multiorder reflection SCs of an IHN BCP PC with EMIMTFSI, we intentionally set up an initial stopband of an IHN BCP PC with the maximum reflectivity at a wavelength of approximately 570 nm. When only 5 weight % (wt %) EMIMTFSI in EtOH/DI water cosolvent was used onto the initial red IHN BCP PC with a commercial spray coater, the second-order reflection peak appeared at approximately 350 nm, as shown in Fig. 3A.

The visible SC of the film was attributed to only the first-order reflection because the second-order one was still in the UV regime, as denoted as group I. With further addition of EMIMTFSI by increasing the number of spraying cycles, both reflections could be located within the visible range, and the second-order reflection dominantly contributed to the SC of the film, giving rise to a SC arising from the mixing of the two reflections, as denoted by group II of Fig. 3A. With five spraying cycles, the third-order reflection moved into the UV regime, and the film showed the three distinct reflections corresponding to the first, second, and third one, as denoted by group III of Fig. 3A. In this case, the visible SC of the film arises dominantly from the second and third reflections, leading to other multiorder SCs. The white-light photographs in Fig. 3B show the various SCs developed from IHN BCP PC as a function of EMIMTFSI covering groups I, II, and III. The preferential absorption of the EMIMTFSI into the IHN-QP2VP domains was confirmed by 2D atomic component mapping of FIB–cross-sectioned IHN BCP PC film with EMIMTFSI using energy-dispersive x-ray spectroscopy (EDX) (fig. S4B).

The multiorder reflection SCs of our IHN BCP PCs with EMIMTFSI were modeled by FDTD (*29*) simulation, and the results are shown in Fig. 3C (fig. S5). The IHN BCP PC was modeled with 12 pairs of alternating PS and IHN-QP2VP layers with initial layer thickness of 45 and 155 nm, respectively. The refractive index of an IHN-QP2VP with EMIMTFSI ($n_{IHN\ IL}$) was calculated by the mean field form $\boldsymbol{n}_{IHN\ IL} = \sqrt{\frac{\boldsymbol{n}^2_{e,o}}{\boldsymbol{\alpha}_{IHN\ IL}} + \boldsymbol{n}^2_{IL}\left(1 - \frac{1}{\boldsymbol{\alpha}_{IHN\ IL}}\right)}$ (*23*) where $n_{e,0}(1.50)$ is the effective refractive index of the initial IHN-QP2VP layer, and $\boldsymbol{\alpha}_{IHN\ IL}$ is the swelling ratio of the IHN-QP2VP domain. The simulation results of an IHN BCP PC with a swelling ratio of $\alpha = 2.4$, shown in Fig. 3D, clearly exhibited the first, second, and third reflections at wavelengths of 1107, 571, and 385 nm, respectively. By varying α, we were able to obtain a full map of multiorder SCs appearing across the UV–visible (vis) near-infrared regime, as shown in Fig. 3C.

The experimental results in Fig. 3A were also plotted as a function of the number of EMIMTFSI spraying cycles, which were directly proportional to the swelling ratio. The results are in good agreement with the simulation results, as shown in Fig. 3C. The results clearly show that our strategy of using multiorder reflections for tuning SCs of BCP PC is pertinent, as schematically shown in

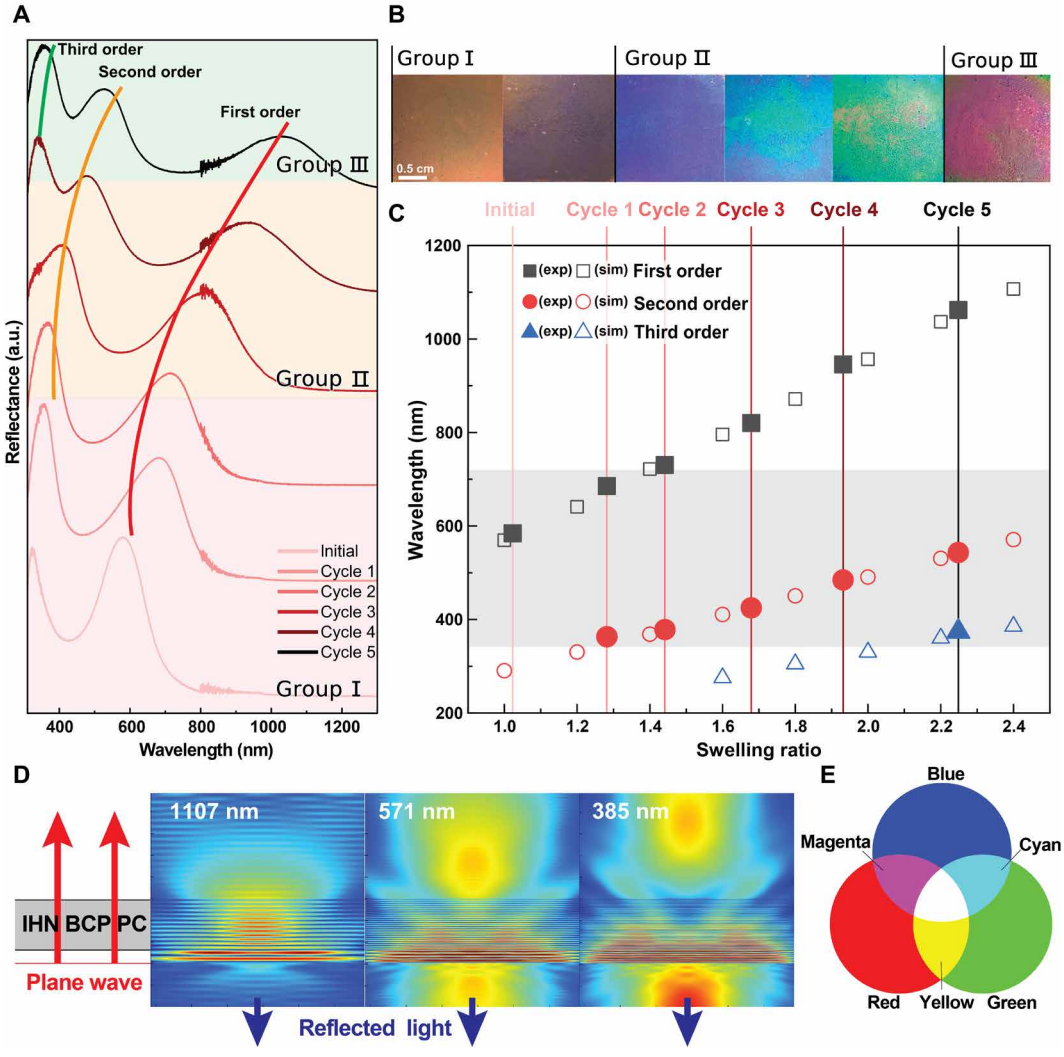

Fig. 3. Multiorder reflections of ionic liquid–doped IHN BCP PC. (**A**) UV-vis spectra of IHN BCP PC films on the glass substrates swollen with 5 wt % EMIMTFSI ink by varying spraying cycles. The films with their SCs arising from the first-order peaks in visible range since the second-order reflection appeared in the UV regime are denoted as group I. The films with their SCs in visible range arising dominantly from second-order reflection are denoted as group II. One with the SC in visible range from the mixing of second- and third-order reflection is denoted as group III. (**B**) Photographs of IHN BCP PC films corresponding to UV-vis spectra in (A). (**C**) FDTD-calculated stopband positions of IHN BCP PCs with various swelling ratios (α). α is defined by domain size of IHN-QP2VP divided by that of IHN-QP2VP with EMIMTFSI. The experimental results of (A) are also plotted with the simulated ones as a function of spraying cycle (solid symbols). (**D**) Representative FDTD simulation results of an IHN BCP PC at a swelling ratio of 2.4. First-, second-, and third-order peaks appear at 1107, 571, 385 nm, respectively. (**E**) Schematic of additive mixing of light. Photo credit: H.S.K., Yonsei University.

Fig. 3E. We also confirmed the pseudoelastic properties of our IHN BCP PCs even after the addition of EMIMTFSI. The nanoindentation results of the IHN BCP PCs with EMIMTFSI show that the effective moduli of all groups I, II, and III range from 200 to 450 MPa and have pseudoelastic properties, as shown in Fig. 2I. As expected, the effective modulus decreased with the increase in the EMIMTFSI content in the film. The temperature stability of an EMIMTFSI-doped IHN BCP PC was examined, and the results show that its $I(q_z)$ was essentially constant with temperature at least up to 160°C (fig. S6).

To obtain a full color display, we used an inkjet printer such that the EMIMTFSI ink was directly deposited onto an IHN BCP PC film, as schematically shown in Fig. 4A. Because the color of the film depends on the amount of EMIMTFSI deposited in a given region (Fig. 3A and fig. S7), the inkjet printer only needs a single ink, which can be deposited onto the IHN BCP PC film. This differs from a commercial inkjet printer, where R, G, and B dye ink from the corresponding ink cartridges create various colors by adjusting the relative amount of the inks. Rather, the black/gray/white contrast with a single EMIMTFSI ink cartridge conveniently produced the SCs of our IHN BCP PC film. An IHN BCP PC film with its maximum reflectance at approximately 350 nm was prepared on an Si substrate, followed by ink jet printing with a black/gray/white contrast. Various SCs covering the entire visible range were successfully developed, as shown in Fig. 4B. A given colored image can be readily produced by our modified EMIMTFSI inkjet printer when the appropriate color information is properly programmed into the black/gray/white contrast. As an example, we converted an image of

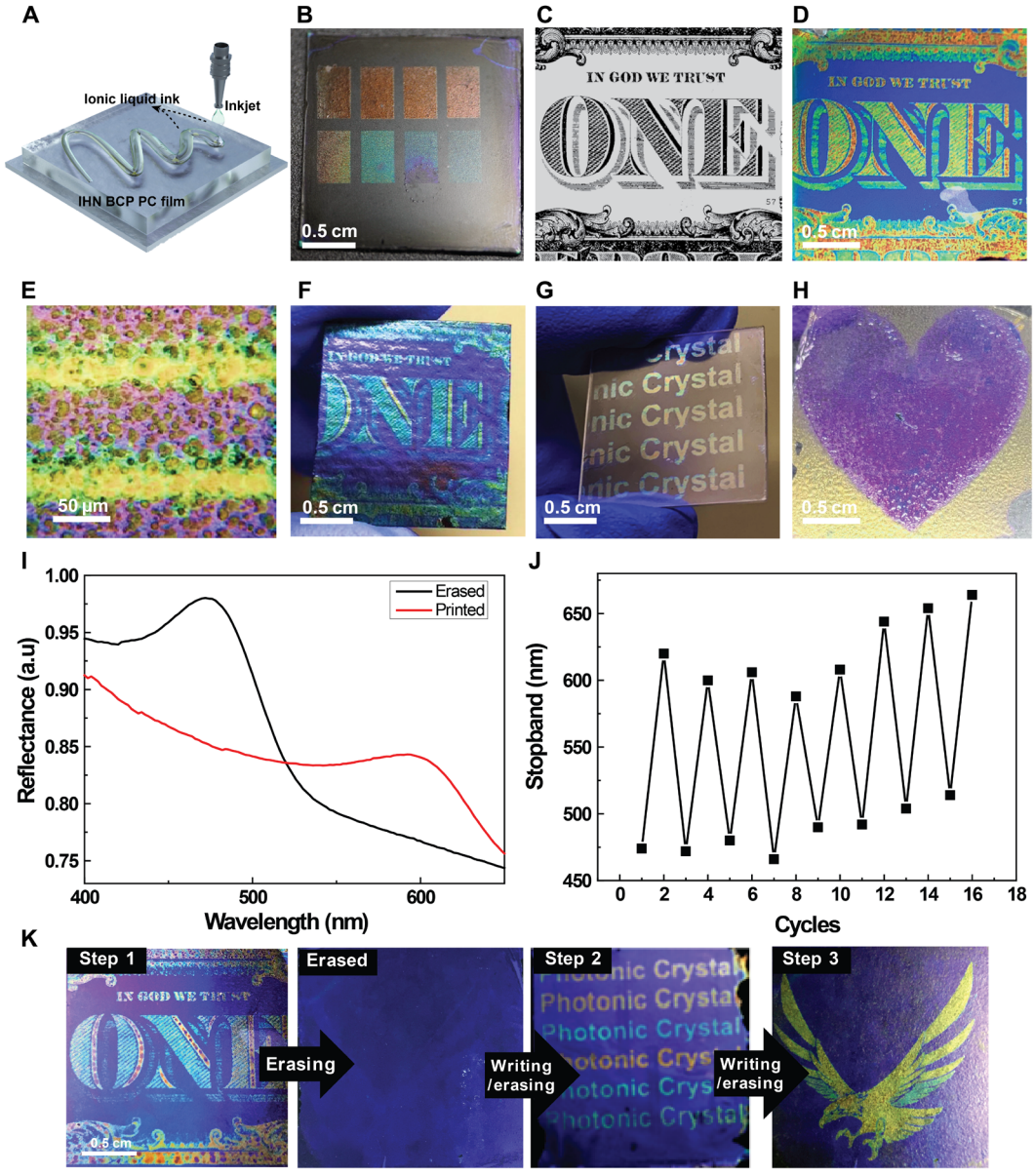

Fig. 4. Printable and rewritable SCs on IHN BCP PC. (**A**) Schematic of inkjet printing on IHN BCP PC film with ionic liquid (IL) ink. (**B**) Photograph of an IL ink-printed IHN BCP PC film with different concentrations. (**C**) Computer-processed image of the part of a one dollar bill in black and white contrast. (**D**) Photograph of the SC image printed by adjusting the concentration of the IL ink based on the contrast image in (C). (**E**) Optical microscope image of lines printed with IL on an IHN BCP PC film, which shows a resolution of the SC lines of approximately 50 μm. Photographs of IL ink-printed SC images of IHN BCP PCs on (**F**) a conventional paper and (**G**) glass substrate. (**H**) Photograph of an IL inkjet-printed image of an IHN BCP PC film arising from multiorder reflection SCs in visible range. (**I**) UV-vis spectra of an IHN BCP PC film printed with IL (red), followed by the removal of the IL by a neat PEGDA pad (black). (**J**) Maximum reflection wavelength values with repetitive IL writing and erasing processes. (**K**) Photographs of different IHN BCP SC images with repetitive printing and erasing of IL ink. An IHN BCP SC image (step 1) inkjet-printed with IL on an IHN BCP PC film, followed by removal of IL with a neat PEGDA pad. The printing and erasing process is repeatable (steps 2 and 3). Photo credit: H.S.K., Yonsei University.

a part of "U.S. one dollar bill" to a black and white contrast image using software, as shown in Fig. 4C. Then, EMIMTFSI inkjet printing on an IHN BCP PC film successfully reconstructed a full color SC image quite similar to the original from the black/gray/white image, as shown in Fig. 4D. The printing speed for 2×2–cm^2 regions is less than 10 s, as fast as that of a conventional office jet printer.

The drop of EMIMTFSI ink wet the film and laterally diffused, defining the pixel size of the printed regions. The printed dot size of commercial ink was measured as approximately 50 μm (fig. S8A). After the viscosity of the EMIMTFSI ink was carefully adjusted to control the wettability of the ink on an IHN BCP PC film, the resolution of our IHN BCP PC film was approximately 60 μm, as shown in Fig. 4E, similar to a commercial ink resolution(~57 μm). Considering the resolution of our printed SC image of approximately 60 μm, the influence of the topological variation (ca. 750 nm) at the interface would not be notable. The resolution was dominantly determined

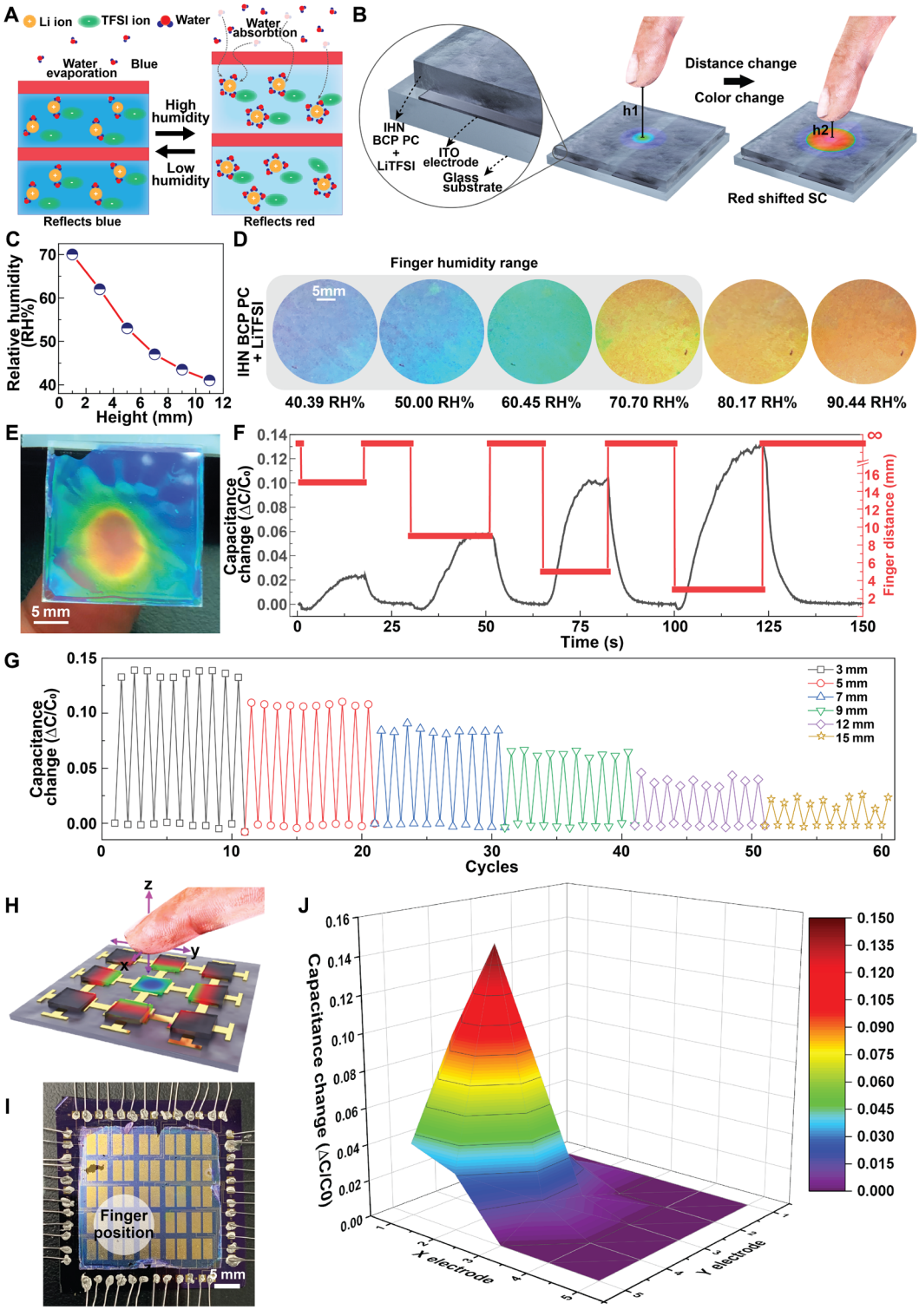

Fig. 5. 3D touchless BCP structural color sensing display. (**A**) Schematic illustration of humidity-sensitive SC change in an LiTFSI-doped IHN BCP PC. (**B**) Schematic of two-terminal parallel-type 3D touchless sensing display with an LiTFSI-doped IHN BCP PC. Height 1 (h1) is higher than height 2 (h2). (**C**) Variation of relative humidity as a function of the finger-to-PC distance. (**D**) Photographs of LiTFSI-doped IHN BCP PCs in various relative humidity conditions from 40 to 90 RH%. (**E**) Photograph showing SC of an LiTFSI-doped IHN BCP PC when a finger is close to the surface. (**F**) Capacitance change of a 3D touchless sensing display with an LiTFSI-doped IHN BCP PC upon variation of finger-to-PC distance from 15, 9, 5, and 3 mm. (**G**) Variation in capacitance of the 3D touchless sensing display upon repetitive alteration of the finger-to-PC distance. Schematic (**H**) and photograph (**I**) of arrays for 3D touchless sensing displays. (**J**) 3D capacitance change map obtained from the arrays of 3D touchless sensing displays with a finger close to the surface of the arrays. Photo credit: H.S.K., Yonsei University.

by lateral diffusion of ionic liquid ink correlated with the size of droplets during printing. Beneficially, our pseudoelastic IHN BCP PC film is easily transferred onto another substrate, allowing for ink-jet printed SC on various substrates. For instance, the printed "one dollar bill" SC image of an IHN BCP PC film that had been on an Si substrate was successfully transferred onto conventional paper, as shown in Fig. 4F. The examples also include the SC images on a glass and a poly(ethylene terephthalate) (Fig. 4G and fig. S9A). A printed SC image arising from the combination of the multiorder reflections (resulting in purple and yellow) was also successfully made, as shown in Fig. 4H.

SCs inkjet printed on our IHN BCP PC film with EMIMTFSI can be erased and rewritten multiple times. To erase an image, the EMIMTFSI inkjetted into an IHN BCP PC was removed by placing an ink absorber, i.e., a neat cross-linked PEGDA gel onto the printed image over 120 s. The jetted EMIMTFSI diffuses out into the hydrogel due to the large concentration gradient of EMIMTFSI developed between the IHN BCP PC and hydrogel layer, allowing the system to reset (fig. S9B). To demonstrate multiple erase/write cycles, we prepared an IHN BCP PC film with a maximum reflectance at approximately 450 nm. The swelling by EMIMTFSI red shifted the maximum to approximately 620 nm (Fig. 4I). After the contact on the swollen film with a neat hydrogel layer for a few minutes, the SC of the film was changed back to the initial state (Fig. 4I). The SC of the IHN BCP PC film was reliably switched for 10 cycles, as shown in Fig. 4J. Figure 4K shows three different full-colored SC images were written and subsequently erased and then rewritten on our flexible and rewritable IHN BCP PC display.

To further use our IHN BCP PC display with the multiorder reflections as a user-interactive 3D touchless sensing display and, in particular, using a humidity-dependent SC variation, we used another ionic liquid ink, *bis*(trifluoromethylsulfonyl)amine lithium salt (LiTFSI), known as one of the most hygroscopic ionic liquids (fig. S4A). When LiTFSI was diffused into an IHN BCP PC, the SC of the PC became sensitive to environmental humidity. Water was readily absorbed into the PC and coordinated with LiTFSI, thickening the IHN-QP2VP domains and giving rise to the red shift of the SC, as schematically shown in Fig. 5A. Because of the characteristic coordination of LiTFSI capable of being associated with water molecules, the SC was readily varied across the visible range as a function of humidity. The system became reversible when water absorbed into IHN BCP PC was diffused out as shown in Fig. 5A. We envisioned that human finger with natural humidity of approximately 90% is an excellent humidity source that could modulate the SC of our IHN BCP PC doped with LiTFSI as a function of finger-to-PC distance, as schematically shown in Fig. 5B. To confirm our speculation, we examined how humidity was varied as a function of the finger-to-PC distance, and the results are shown in Fig. 5C. The humidity was changed from approximately 70 to 40 RH% (ambient relative humidity) when the distance was altered from 1 to 15 mm from the surface of our LiTFSI-doped IHN BCP PC, giving rise to the SC variation from blue, green, to orange.

On the basis of the results of the humidity-dependent SC variation in Fig. 5D, we were able to develop a 3D touchless interactive display where z axis finger information was monitored with the variation of capacitance as well as SC, as schematically shown in Fig. 5B. An LiTFSI-doped IHN BCP PC was transferred onto two parallel indium tin oxide (ITO) electrodes, which could monitor the capacitance change of the PC depending upon the moisture uptake. Four sequential finger positions along the z axis with different finger-to-the PC distance were monitored with both capacitance, and SC change and the results are shown in Fig. 5 (E and F). When a finger was close to the surface, the capacitance was increased because of high water uptake, also giving rise to the red shift of the SC of our LiTFSI-doped IHN BCP PC. The SC variation upon the four finger positions was shown in the gray box of Fig. 5D. The SC was varied from blue, green, to orange when a finger approached the surface of the PC.

Our 3D touchless sensing display successfully worked under multiple sensing events with different finger-to-the PC distances, and the results in Fig. 5G showed that each 3D location along the z axis was distinguished repetitively in capacitance change. It should be noted that an IHN BCP PC without LiTFSI also responded to humidity because of hygroscopic characteristics of IHN, but the device became less sensitive to environmental humidity. The response time for the capacitance increase arising from water uptake was approximately 20 s, while that for the capacitance decrease ascribed to the removal of the water was less than approximately 10 s. For precise 3D recognition of a finger hovering in the x, y, and z directions, we further fabricated arrays of 3D touchless sensing displays, as shown in Fig. 5, H and I. First, arrays of pairs of ITO parallel electrodes were developed on a glass substrate, followed by depositing an LiTFSI-doped IHN BCP PC film (fig. S8B). When a finger was located at the bottom left area of the sensing display arrays, the 3D position information of the finger was readily reconstructed in capacitance change, as shown in Fig. 5J. The reversible change in SC was quite sustainable even after 55-time cycles (fig. S10). Because our sensing display is based on water diffusion into IHN BCP PC, the sensitivity of the humidity would decrease with the film thickness.

DISCUSSION

We demonstrated a user-interactive 3D touchless sensing display based on BCP PCs with IHN. Facile expansion of a BCP PC microdomain was achieved by using chemically cross-linked IHN in the BCP PC microdomains, giving rise to mechanically soft but robust full-visible-range SCs with an effective modulus of a few hundred MPa. When a nonvolatile ionic liquid swelling agent was absorbed into the domains of the interpenetrated network, not only first-order but also second- and third-order photonic reflections appeared in the visible regime, giving rise to richer visible SCs arising from two color mixing of pairs of reflections. By combining with various ionic liquid dopants as printing inks, our pseudo solid-state IHN BCP PCs with multiorder reflection SC were successfully used for printable and rewritable displays as well as 3D touchless sensing displays where finger approach (z) and lateral position (x and y) were precisely monitored via capacitance and SC change, demonstrating a new approach for emerging solid-state sensors and displays.

MATERIALS AND METHODS

Material

A PS-*b*-P2VP was synthesized via living anionic polymerization (*36*). The number average molecular weight of the PS-*b*-P2VP BCP was 126 kg mol^{-1} [Φ_{ps} = 0.49, polymer dispersity index (PDI) = 1.05]. PGMEA, chloroform, ethanol, PEGDA (M_n = 700), HOMPP, Triton

X-100, EMIMTFSI, LiTFSI, bromoethane, 1,4-dibromobutane, and hydrobromic acid were purchased from Sigma-Aldrich.

Preparation of BCP PC films

BCP PC films were fabricated by spin coating PS-*b*-P2VP solutions (7 wt %, in PGMEA) onto glass substrates, and then solvent annealed in chloroform vapor at 50°C for 12 hours. After that, P2VP layers were selectively quaternized using 1-bromoethane and 1,4-dibromobutane in hexane at 60°C for 24 hours. The initial SC of a BCP PC film is controlled by the degree of cross-linking with the amount of 1,4-dibromobutane (*19*, *23*).

Preparation of IHN BCP PC films

PEGDA (M_n = 700) solution (50 wt % in DI water) was prepared with HOMPP and Triton X-100. HOMPP was added to the solution with 1.5 wt % to cross-linking acrylate of the PEGDA chains. Triton X-100 was used to control the wettability and diffusion rate suitable for uniformly PEGDA swollen PS-*b*-P2VP lamellar structure.

Addition of EMIMTFSI by increasing the spraying cycles

EMIMTFSI was dissolved in an ethanol. For further addition of EMIMTFSI to IHN BCP PC, 5 wt % of EMIMTFSI ethanol solution was used. The spray coating process was performed with a spray coater (laboratory spray coater, ReVo-S).

Preparation of EMIMTFSI for printable display

EMIMTFSI was dissolved in a cosolvent (DI water and ethanol). For inkjet printing with a commercial printer (PIXMA iP7270, Canon), 10 wt % EMIMTFSI (DI water:ethanol = 1:1) solution was used.

Preparation of 3D touchless sensing display with LiTFSI ink

LiTFSI was dissolved in a cosolvent (DI water and ethanol). For inkjet printing LiTFSI in an IHN BCP PC film with a commercial printer (PIXMA iP7270, Canon), 10 wt % LiTFSI (DI water:ethanol = 1:1) solution was used. LiTFSI-doped IHN BCP PC was placed on arrays of pairs of two parallel ITO electrodes sputtered with a pattern mask fabricated by photolithography, giving rise to the 5 × 5 arrays of 3D touchless sensing displays.

Characterization

The cross-sectional images of in-plane lamellar structures of IHN BCP PC films were imaged by bright-field TEM and EDX with spherical aberration (Cs)–corrected spherical aberration-corrected scanning TEM (JEM-ARM 200F, JEOL). Thin cross sections of dried films were prepared by an FIB (JIB-4601F, JEOL). GISAXS measurements were performed on IHN BCP PC films, which have stopbands in red, green, and blue, and the EMIMTFSI printed sample using the PLS-II 9A U-SAXS beamline at the Pohang Accelerator Laboratory. UV-vis spectra were measured using a UV-vis spectrometer (Cary 5000, Agilent). Optical microscope images were used to observe the printed SC films (BX 51 M, Olympus). The mechanical properties of SC film samples were measured by using the ultra nanohardness indentation tester (CSM Instrument). FDTD simulation was performed using DEVICE Multiphysics Simulation Suite (Lumerical Inc.). The simulation was carried out under the condition that a plane wave having a wavelength of 200 to 2.5 nm was incident perpendicularly to the modeled EMIMTFSI swollen IHN BCP PC. Uniaxial anisotropic perfectly matched layer boundary condition was used during the simulation.

SUPPLEMENTARY MATERIALS

Supplementary material for this article is available at http://advances.sciencemag.org/cgi/content/full/6/30/eabb5769/DC1

REFERENCES AND NOTES

1. W. Gao, S. Emaminejad, H. Y. Y. Nyein, S. Challa, K. Chen, A. Peck, H. M. Fahad, H. Ota, H. Shiraki, D. Kiriya, D.-H. Lien, G. A. Brooks, R. W. Davis, A. Javey, Fully integrated wearable sensor arrays for multiplexed in situ perspiration analysis. *Nature* **529**, 509–514 (2016).
2. T.-P. Huynh, H. Haick, Autonomous flexible sensors for health monitoring. *Adv. Mater.* **30**, e1802337 (2018).
3. A. C. Arsenault, T. J. Clark, G. von Freymann, L. Cademartiri, R. Sapienza, J. Bertolotti, E. Vekris, S. Wong, V. Kitaev, I. Manners, R. Z. Wang, S. John, D. Wiersma, G. A. Ozin, From colour fingerprinting to the control of photoluminescence in elastic photonic crystals. *Nat. Mater.* **5**, 179–184 (2006).
4. D. Yang, S. Ye, J. Ge, From metastable colloidal crystalline arrays to fast responsive mechanochromic photonic gels: An organic gel for deformation-based display panels. *Adv. Funct. Mater.* **24**, 3197–3205 (2014).
5. S. W. Lee, S. H. Cho, H. S. Kang, G. Kim, J. S. Kim, B. Jeong, E. H. Kim, S. Yu, I. Hwang, H. Han, T. H. Park, S.-H. Jung, J. K. Lee, W. Shim, C. Park, Electroluminescent pressure-sensing displays. *ACS Appl. Mater. Interfaces* **10**, 13757–13766 (2018).
6. T. H. Park, S. Yu, S. H. Cho, H. S. Kang, Y. Kim, M. J. Kim, H. Eoh, C. Park, B. Jeong, S. W. Lee, D. Y. Ryu, J. Huh, C. Park, Block copolymer structural color strain sensor. *NPG Asia Mater.* **10**, 328–339 (2018).
7. E. H. Kim, H. Han, S. Yu, C. Park, G. Kim, B. Jeong, S. W. Lee, J. S. Kim, S. Lee, J. Kim, J.-U. Park, W. Shim, C. Park, Interactive skin displays: Interactive skin display with epidermal stimuli electrode. *Adv. Sci.* **6**, 1802351 (2019).
8. Y. Y. Diao, X. Y. Liu, G. W. Toh, L. Shi, J. Zi, Multiple structural coloring of silk-fibroin photonic crystals and humidity-responsive color sensing. *Adv. Funct. Mater.* **23**, 5373–5380 (2013).
9. E. H. Kim, S. H. Cho, J. H. Lee, B. Jeong, R. H. Kim, S. Yu, T.-W. Lee, W. Shim, C. Park, Organic light emitting board for dynamic interactive display. *Nat. Commun.* **8**, 14964 (2017).
10. H.-H. Chou, A. Nguyen, A. Chortos, J. W. F. To, C. Lu, J. Mei, T. Kurosawa, W.-G. Bae, J. B.-H. Tok, Z. Bao, A chameleon-inspired stretchable electronic skin with interactive colour changing controlled by tactile sensing. *Nat. Commun.* **6**, 8011 (2015).
11. H. Park, D. S. Kim, S. Y. Hong, C. Kim, J. Y. Yun, S. Y. Oh, S. W. Jin, Y. R. Jeong, G. T. Kim, J. S. Ha, A skin-integrated transparent and stretchable strain sensor with interactive color-changing electrochromic displays. *Nanoscale* **9**, 7631–7640 (2017).
12. G. Kim, S. Cho, K. Chang, W. S. Kim, H. Kang, S.-P. Ryu, J. Myoung, J. Park, C. Park, W. Shim, Spatially pressure-mapped thermochromic interactive sensor. *Adv. Mater.* **29**, 1606120 (2017).
13. T. Bu, T. Xiao, Z. Yang, G. Liu, X. Fu, J. Nie, T. Guo, Y. Pang, J. Zhao, F. Xi, C. Zhang, Z. L. Wang, Stretchable triboelectric–photonic smart skin for tactile and gesture sensing. *Adv. Mater.* **30**, e1800066 (2018).
14. X. Y. Wei, X. Wang, S. Y. Kuang, L. Su, H. Y. Li, Y. Wang, C. Pan, Z. L. Wang, G. Zhu, Dynamic triboelectrification-induced electroluminescence and its use in visualized sensing. *Adv. Mater.* **28**, 6656–6664 (2016).
15. S. H. Cho, J. Sung, I. Hwang, R. H. Kim, Y. S. Choi, S. S. Jo, T. W. Lee, C. Park, High performance AC electroluminescence from colloidal quantum dot hybrids. *Adv. Mater.* **24**, 4540–4546 (2012).
16. C. H. Yang, B. H. Chen, J. X. Zhou, Y. M. Chen, Z. G. Suo, Electroluminescence of giant stretchability. *Adv. Mater.* **28**, 4480–4484 (2016).
17. G. Isapour, M. Lattuada, Bioinspired stimuli-responsive color-changing systems. *Adv. Mater.* **30**, e1707069 (2018).
18. J.-H. Lee, C. Y. Koh, J. P. Singer, S.-J. Jeon, M. Maldovan, O. Stein, E. L. Thomas, 25th anniversary article: Ordered polymer structures for the engineering of photons and phonons. *Adv. Mater.* **26**, 532–569 (2014).
19. Y. Kang, J. J. Walish, T. Gorishnyy, E. L. Thomas, Broad-wavelength-range chemically tunable block-copolymer photonic gels. *Nat. Mater.* **6**, 957–960 (2007).
20. H. Li, C. Li, W. Sun, Y. Wang, W. Hua, J. Liu, S. Zhang, Z. Chen, S. Wang, Z. Wu, Q. Zhu, R. Tang, J. Yu, L. He, G. A. Ozin, X. Zhang, Single-stimulus-induced modulation of multiple optical properties. *Adv. Mater.* **31**, e1900388 (2019).
21. S. Y. Lee, J.-S. Lee, S.-H. Kim, Colorimetric recording of thermal conditions on polymeric inverse opals. *Adv. Mater.* **31**, 1901398 (2019).

22. T. M. Choi, K. Je, J.-G. Park, G. H. Lee, S.-H. Kim, Photonic capsule sensors with built-in colloidal crystallites. *Adv. Mater.* **30**, e1803387 (2018).
23. H. S. Kang, J. Lee, S. M. Cho, T. H. Park, M. J. Kim, C. Park, S. W. Lee, K. L. Kim, D. Y. Ryu, J. Huh, E. L. Thomas, C. Park, Printable and rewritable full block copolymer structural color. *Adv. Mater.* **29**, 1700084 (2017).
24. T. J. Park, S. K. Hwang, S. Park, S. H. Cho, T. H. Park, B. Jeong, H. S. Kang, D. Y. Ryu, J. Huh, E. L. Thomas, C. Park, Electrically tunable soft-solid block copolymer structural color. *ACS Nano* **9**, 12158–12167 (2015).
25. J. J. Walish, Y. Kang, R. A. Mickiewicz, E. L. Thomas, Bioinspired electrochemically tunable block copolymer full color pixels. *Adv. Mater.* **21**, 3078–3081 (2009).
26. K. Hwang, D. Kwak, C. Kang, D. Kim, Y. Ahn, Y. Kang, Electrically tunable hysteretic photonic gels for nonvolatile display pixels. *Angew. Chemie. Int. Ed.* **50**, 6311–6314 (2011).
27. E. Kim, C. Kang, H. Baek, K. Hwang, D. Kwak, E. Lee, Y. Kang, E. L. Thomas, Control of optical hysteresis in block copolymer photonic gels: A step towards wet photonic memory films. *Adv. Funct. Mater.* **20**, 1728–1732 (2010).
28. H. Eoh, H. S. Kang, M. J. Kim, M. Koo, T. H. Park, Y. Kim, H. Lim, D. Y. Ryu, E. Kim, J. Huh, Y. Kang, C. Park, Nonvolatile, multicolored photothermal writing of block copolymer structural color. *Adv. Funct. Mater.* **29**, 1904055 (2019).
29. Y. Fan, J. J. Walish, S. Tang, B. D. Olsen, E. L. Thomas, Defects, solvent quality, and photonic response in lamellar block copolymer gels. *Macromolecules* **47**, 1130–1136 (2014).
30. K. Yee, Numerical solution of initial boundary value problems involving Maxwell's equations in isotropic media. *IEEE Trans. Antennas Propag.* **14**, 302–307 (1966).
31. W. C. Oliver, G. M. Pharr, An improved technique for determining hardness and elastic modulus using load and displacement sensing indentation experiments. *J. Mater. Res.* **7**, 1564–1583 (1992).
32. H. J. Kim, D. E. Kim, Effects of proximity on hardness and elastic modulus measurements of SiO_2 and Cu by nanoindentation. *Tribol. Lett.* **49**, 85–94 (2013).
33. K. Hanna, O. Yasar-Inceoglu, O. Yasar, Drug delivered poly (ethylene glycol) diacrylate (PEGDA) hydrogels and their mechanical characterization tests for tissue engineering applications. *MRS Adv.* **3**, 1697–1702 (2018).
34. V. Chan, P. Zorlutuna, J. H. Jeong, H. Kong, R. Bashir, Three-dimensional photopatterning of hydrogels using stereolithography for long-term cell encapsulation. *Lab Chip* **10**, 2062–2070 (2010).
35. A. Zellander, A. Kadakia-Bhasin, M. Mahksous, M. Cho, Mechanical diversity of porous poly (ethylene glycol) diacrylate. *Adv. Biomed. Eng. Res.* **1**, 9–15 (2013).
36. S. Park, K. Koo, K. Kim, H. Ahn, B. Lee, C. Park, D. Y. Ryu, Transition behavior of asymmetric polystyrene-*b*-poly (2-vinylpyridine) films: A stable hexagonally modulated layer structure. *Polymer* **60**, 32–39 (2015).

Acknowledgments
Funding: This research was supported by grants from the National Research Foundation of Korea (NRF) funded by the Korean government (MEST) (nos. 2017R1A2A1A05001160, 2017M3D1A1039289, and 2018M3D1A1058536). This work was also supported by the KIST Institutional Program (project no. 2Z05900-19-P096). **Author contributions:** Che.P., W.-G.K., and H.S.K. conceived and designed the experiments. H.S.K., S.W.H., and H.E. performed the cross-linking and fabrication of the IHN BCP PC film. Cha.P., S.W.L., and T.H.P. performed the morphology characterization. D.Y.R. synthesized BCPs. J.B., D.-G.S., H.L., and D.-E.K. measured the mechanical property of the films. Che.P., W.G.K., J.H., and E.L.T. supervised the project, analyzed the data, and wrote the paper. All authors discussed the results and commented on the paper. **Competing interests:** Che.P. and H.S.K. are inventors on a patent application related to this work filed with the Korean Intellectual Property Office by Yonsei University (no. 10-2019-0042288, filed 11 May 2019). The authors declare that they have no other competing interests. **Data and materials availability:** All data needed to evaluate the conclusions in the paper are present in the paper and/or the Supplementary Materials. Additional data related to this paper may be requested from the authors.

Submitted 24 Feb 2020
Accepted 11 June 2020
Published 22 July 2020
10.1126/sciadv.abb5769

Citation: H. S. Kang, S. W. Han, C. Park, S. W. Lee, H. Eoh, J. Baek, D.-G. Shin, T. H. Park, J. Huh, H. Lee, D.-E. Kim, D. Y. Ryu, E. L. Thomas, W.-G. Koh, C. Park, 3D touchless multiorder reflection structural color sensing display. *Sci. Adv.* **6**, eabb5769 (2020).